CLIMATOLOGY

Repetitive mammalian dwarfing during ancient greenhouse warming events

Abigail R. D'Ambrosia,[1]* William C. Clyde,[1] Henry C. Fricke,[2] Philip D. Gingerich,[3] Hemmo A. Abels[4]

Abrupt perturbations of the global carbon cycle during the early Eocene are associated with rapid global warming events, which are analogous in many ways to present greenhouse warming. Mammal dwarfing has been observed, along with other changes in community structure, during the largest of these ancient global warming events, known as the Paleocene-Eocene Thermal Maximum [PETM; ~56 million years ago (Ma)]. We show that mammalian dwarfing accompanied the subsequent, smaller-magnitude warming event known as Eocene Thermal Maximum 2 [ETM2 (~53 Ma)]. Statistically significant decrease in body size during ETM2 is observed in two of four taxonomic groups analyzed in this study and is most clearly observed in early equids (horses). During ETM2, the best-sampled lineage of equids decreased in size by ~14%, as opposed to ~30% during the PETM. Thus, dwarfing appears to be a common evolutionary response of some mammals during past global warming events, and the extent of dwarfing seems related to the magnitude of the event.

INTRODUCTION

Climate change affects plants and animals in ways that are poorly understood. Much can be learned from the study of climate change in the geological past and its effect on contemporaneous biotas. Early Eocene global warming events, or "hyperthermals," are associated with large perturbations of the global carbon cycle and thus serve as analogs of modern-day global warming. The largest of the hyperthermals was the Paleocene-Eocene Thermal Maximum (PETM), which occurred approximately 56 million years ago (Ma) and lasted about 180,000 years (*1*, *2*). The PETM is recognized in the geological record by marine and terrestrial carbon isotope excursions (CIEs) of about −3 per mil (‰) and −3 to −6‰ (*2*–*4*), respectively, and an increase in global temperatures of 5° to 8°C within 10,000 years (*2*, *5*, *6*).

Consequences of the PETM's rapid shifts in carbon cycling and atmospheric temperatures were recorded in both marine and terrestrial records, including profound biotic turnover and ecologic change in the terrestrial realm. One of the most extensively studied terrestrial records of the PETM is located in the Bighorn Basin of Wyoming. Here, the event is characterized by transient changes in vegetative composition, from warm temperate paleofloras to those that are indicative of dry tropical and subtropical climates (*2*). Terrestrial records of the PETM are also accompanied by significant mammalian turnover, including the abrupt introduction of several modern mammalian lineages (including perissodactyls, artiodactyls, and primates) and mammalian dwarfing in both immigrant and endemic taxa, observed through changes in the size of fossilized adult teeth [we use the term "dwarfing" to simply describe an observed size decrease, whether it be an evolutionary response or a response that involves other processes as well (for example, migration and ecophenotypic change)] (*7*–*11*). Since the discovery of the PETM in deep-sea cores and continental sections, subsequent smaller-magnitude CIEs have also been discovered in marine records (*12*, *13*). The second largest hyperthermal of the early Eocene, known as ETM2, occurred about 2 million years after the PETM (approximately 53.7 Ma) and was associated with a deep-sea CIE of >1.4‰ and ~3°C warming (*12*, *13*)—about half the magnitude of the PETM (*13*). Another smaller-amplitude hyperthermal, identified as "H2," appears in the marine record about 100,000 years after ETM2 (approximately 53.6 Ma), with a CIE of ~0.8‰ and ~2°C warming (*13*).

More recently, geochemical evidence of ETM2 and H2 was uncovered in terrestrial sedimentary deposits within the Bighorn Basin, with CIEs of −3.8 and −2.8‰, respectively (*14*, *15*). However, their effects on terrestrial climates and ecosystems are not yet documented. Preliminary results indicated that these hyperthermals were not associated with previously identified mammalian turnover events [(*14*); see the study of Chew (*16*) for a suggestion of turnover within this interval in the southern Bighorn Basin], and no detailed study has yet been carried out investigating within-lineage mammalian body size change as done for the PETM (*17*).

Using the newly documented terrestrial records of ETM2 and H2, this study addresses two important questions: (i) Similar to the PETM, is mammalian body size change also found in association with ETM2 and H2? If so, (ii) is there a relationship between the magnitude of a hyperthermal and/or carbon cycle perturbation and the degree of mammalian dwarfing? Understanding the similarities and differences between biotic responses to the PETM and these other smaller hyperthermals is important for determining what kinds of biological responses might be typical for rapid global warming events like what we are experiencing today.

Mammalian fossils used in this study were collected from localities within the northern Bighorn Basin of Wyoming that stratigraphically span known locations of the ETM2 and H2 CIEs. The Bighorn Basin is located in northwestern Wyoming, approximately 130 km east of Yellowstone National Park (Fig. 1). The basin formed during the Laramide orogeny and is bordered by the Beartooth Mountains to the northwest, Bighorn Mountains to the east, and Owl Creek Mountains to the south. It is composed of up to 4500 m of stratigraphically continuous synorogenic continental sedimentary deposits that accumulated through the early Paleogene (*18*–*20*). The fossils in this study are from the Willwood Formation, which is composed dominantly of channel sandstones and brightly colored pedogenically modified overbank mudstone deposits (paleosols), suggesting paleoenvironments of open-canopy forests and relatively dry floodplains (*21*, *22*). Aside from numerous fossil mammals, the Willwood Formation also preserves fossil reptiles, birds, amphibians,

[1]Department of Earth Sciences, University of New Hampshire, 56 College Road, Durham, NH 03824, USA. [2]Department of Geology, Colorado College, 14 East Cache La Poudre Street, Colorado Springs, CO 80903, USA. [3]Museum of Paleontology and Department of Earth and Environmental Sciences, University of Michigan, Ann Arbor, MI 48109, USA. [4]Department of Geosciences and Engineering, Delft University of Technology, Stevinweg 1, 2628 CN Delft, Netherlands.
*Corresponding author. Email: adambrosia@gmail.com

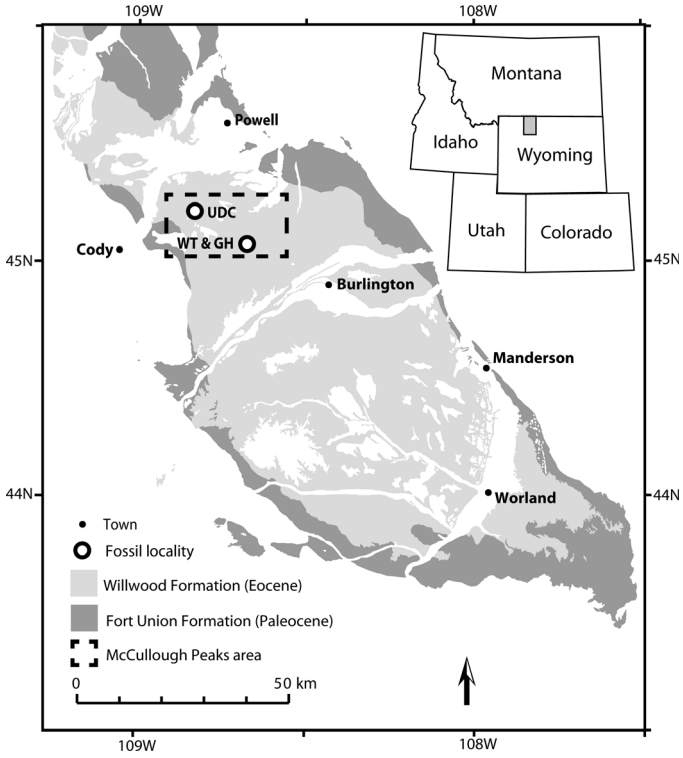

Fig. 1. Bighorn Basin and sample localities. The Bighorn Basin is located in northwestern Wyoming, USA. Upper Deer Creek (UDC), Gilmore Hill (GH), and White Temple (WT) stratigraphic sections are located within the McCullough Peaks region of the northern Bighorn Basin (outlined by a dashed box, see close-up in fig. S1).

and plants (*18*). The early Cenozoic began with minimal-to-no polar ice caps and high global temperatures that reached their long-term peak during the Early Eocene Climatic Optimum (~52 to 50 Ma) (*23*). Within the Bighorn Basin, atmospheric mean annual temperatures during the PETM were estimated to reach between 19° and 26°C (*2*, *6*, *24*).

The thick, stratigraphically continuous [on 100,000-year to 400,000-year time scales; (*15*)] deposits of the Bighorn Basin have long promoted high-resolution studies of ecology, evolutionary trends in flora and fauna, and most recently, past climate (*2*, *25*, *26*). Since the early 1990s, stable carbon isotope studies of pedogenic carbonates have been conducted in the paleosols of the basin to develop continental records of hyperthermal CIEs (*14*, *15*, *27*–*29*). The carbon isotopic composition of pedogenic carbonate is useful for recording CIEs because soil CO_2, from which the carbonate precipitates, ultimately tracks atmospheric $\delta^{13}C$ (*27*). Today, soil CO_2 at depths greater than ~30 cm is dominantly a product of root respiration and within-soil organic matter decomposition because atmospheric CO_2 has an insignificant direct influence at this depth (*30*, *31*). Combining a ~4.4‰ ^{13}C enrichment (relative to plant tissue) through diffusion of CO_2 to the atmosphere with an enrichment of ~10.5‰ due to temperature-dependent carbonate precipitation fractionations, the $\delta^{13}C$ of soil carbonates today mirror the $\delta^{13}C$ of overlying flora with an offset of ~−15‰ (*28*, *30*, *31*). Because pCO_2 may have changed over time, it should be noted that these ^{13}C enrichment values are present-day estimates (*32*–*34*). Carbonate nodules will form when high soil CO_2 production and organic decay lead to acidic solutions that leach the upper part of the soil. These fluids percolate down into the soil and, in combination with an increase in the concentration of Ca^{2+} or pH, promote calcite precipitation (*30*).

Through the use of carbon isotope analyses of pedogenic carbonate, ETM2 and H2 have recently been identified in the McCullough Peaks region of the northern Bighorn Basin (fig. S1). Five stratigraphic sections now capture the ETM2 and H2 CIEs in this area—GH (Gilmore Hill), WT (White Temple), UDC (Upper Deer Creek), WB (West Branch), and CSH (Creek Star Hill). GH and UDC were first reported by Abels *et al.* (*14*), WB and CSH were first reported by Abels *et al.* (*15*), and WT is newly described in this study. This study also provides an updated, higher-resolution, GH isotope section that leads to a revised correlation between GH and UDC. Our updated version of the GH isotope section integrates both the new data and the previous data by Abels *et al.* (*14*). The stratigraphic sections are correlated via tracing of stratigraphic horizons, including a distinct purple marker bed known as Purple 2 [P2; first identified by Abels *et al.* (*14*), which lies in the center of the ETM2 CIE in all sections; Fig. 2 and fig. S2]. The correlation of these sites has also been constrained through magnetostratigraphy and correlation of the CIEs (*14*, *15*). In addition, precession and eccentricity scale patterns from the McCullough Peaks CIEs are very similar to marine CIE patterns, further confirming correlations between sections (*15*).

Stable isotopes of fossil mammal tooth enamel were analyzed to complement the paleosol carbonate analyses, to confirm the stratigraphic position of specimens within the CIEs, and to investigate the paleoecology of these extinct taxa. Because of the precipitation of mammal tooth enamel during ontogenesis, certain teeth may serve as records of an organism's paleoecology, including isotopic information about ingested water and consumed vegetation. This is possible because tooth enamel is composed of bioapatite, $Ca_5(PO_4, CO_3)_3(OH, CO_3)$, which precipitates in equilibrium with body water (*35*–*37*). Furthermore, in terms of preservation, enamel is more resistant to recrystallization and postmortem diagenesis than is bone or dentine because of comparatively smaller amounts of collagen and a larger crystal size (*38*, *39*).

Carbon isotopes in tooth enamel of noncarnivores reflect the $\delta^{13}C$ of consumed vegetation, which tracks $\delta^{13}C_{atmosphere}$ through isotopic fractionation processes associated with photosynthesis (*33*, *39*, *40*). Oxygen isotopes in mammalian body water ultimately record the isotopic values of ingested meteoric water and, with the use of established physical models for a range of mammal sizes, can be used to estimate $\delta^{18}O_{meteoric\ water}$, which is in turn linked to local atmospheric temperature (*35*–*37*, *39*, *41*).

Using tooth size as a proxy for body size, evidence for mammalian dwarfing has been recorded in terrestrial records of the PETM (*7*, *8*, *10*). Teeth in adult mammals scale proportionally to body size. Of all tooth positions, the first lower molar (M_1) tends to exhibit the strongest correlation between crown area and body weight across most taxonomic groups of mammals. However, the crown area of other molars are also highly correlated with body size (see Materials and Methods for further discussion of body size calculations) (*42*–*44*). A high-resolution study focusing on the earliest equid *Sifrhippus* demonstrated a decrease of at least 30% in body size during the first 130,000 years of the PETM, followed by a 76% rebound in body size during the recovery phase of the PETM. It is possible that the PETM records begin on an unconformity within the central and southern Bighorn Basin, and as a result, early PETM fossil records may not encapsulate the true extent of dwarfism. Assuming pre- and post-PETM environmental conditions were equal, pre- and post-PETM body size could also be assumed as equal. In this case, on the basis of a comparison between mid- and post-PETM body size cited in the high-resolution study of Secord *et al.* (*10*), the extent of early equid PETM dwarfing may have reached ~44%.

For the purpose of comparison, our ETM2 and H2 study focuses on body size change in the early equid lineage *Arenahippus pernix* (see

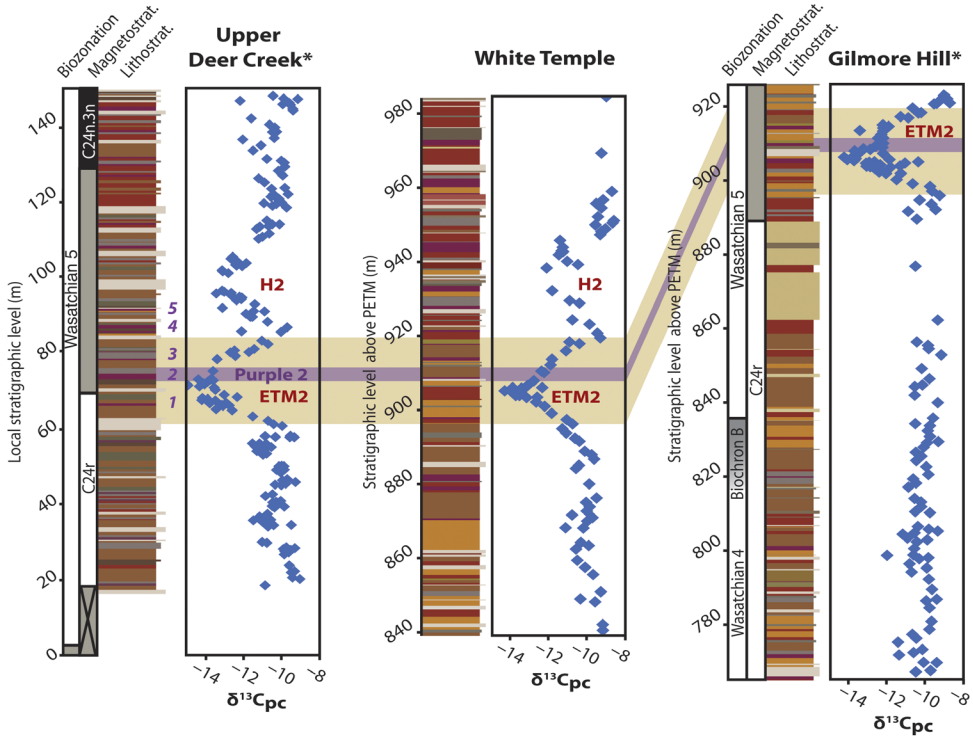

Fig. 2. Stratigraphic framework. Lithostratigraphy, paleosol carbonate nodule isotope stratigraphy ($\delta^{13}C_{pc}$), biozonation, and magnetostratigraphy of the GH, WT, and UDC sections. The tan-shaded region highlights the body of ETM2 across all sections. The purple band represents the P2 marker bed, which can be visually traced across all outcrop sections in the field, and is associated with the most negative values of the ETM2 CIE. *Modified from Abels *et al.* (*14*).

Materials and Methods for note on taxonomy). Fossils of early equids are common in lower Eocene deposits of the Bighorn Basin, making a comparison between the PETM and ETM2 hyperthermal events possible. This study further investigates three other commonly occurring mammalian lineages: *Diacodexis metsiacus*, an early rabbit-sized artiodactyl that had cursorial/saltatorial locomotive adaptations (*45*); *Hyopsodus simplex*, a generalist herbivorous archaic ungulate with weasel-like body proportions (*45*); and *Cantius abditus*, an early frugivorous primate similar to modern lemurs (*45*), although sample sizes for these three lineages were less favorable.

RESULTS

The carbon isotope values in paleosol carbonate ($\delta^{13}C_{pc}$) at WT range from −14.3‰ to −8.6‰, and the average is −10.9‰. There are two distinct and well-defined excursions reaching −13.7‰ at 905.3 m above the PETM [based on a five-point moving average with a 95% confidence interval (CI) of −14.0 to −13.3] and −11.3‰ at 938.8 m above the PETM (95% CI, −11.9 to −10.7) (Figs. 2 and 3A and table S1). These two CIEs at WT can be confidently correlated to the ETM2 and H2 CIEs in the Deer Creek area of the McCullough Peaks (*14*, *15*). The distinct P2 marker bed that falls within the lower isotope excursion at WT can be traced to the ETM2 CIE through WB, CSH, and UDC (Fig. 2). The smaller excursion that falls 33.5 m above the larger excursion at WT is similar in magnitude to H2 at UDC, which falls 24.6 m above the ETM2 in that section.

Isotopic analyses of the newly sampled GH section carbonate nodules resulted in a minimum $\delta^{13}C$ of −13.5‰ (based on a five-point moving average; 95% CI, −14.3 to −12.7) at the 906.1-m level and a maximum $\delta^{13}C$ of −9.0‰ (95% CI, −9.2 to −8.7) at the 921.1-m level (Fig. 2, fig. S3, and table S2). The previous GH minimum $\delta^{13}C$ was reported as −12.0‰ and the maximum as −8.7‰ (fig. S3) (*14*). The updated $\delta^{13}C$ minimum of −13.5‰ occurs within 2.7 m of P2 and thus clearly represents the ETM2 CIE [and not the H2 CIE as originally proposed by Abels *et al.* (*14*)]. These new isotopic and lithostratigraphic data now clearly show the stratigraphic expression of ETM2 and H2 across the entire McCullough Peaks escarpment (Fig. 2). In addition, $\delta^{13}C$ of *Arenahippus* tooth enamel from GH and WT exhibited the lowest values of −15.0‰ at 910.4 m, within the ETM2 CIE, indicating that these fossils are in fact associated with the hyperthermal events identified in the surrounding paleosol carbonate nodule records (Fig. 3B and table S3). Although $\delta^{18}O$ of the same *Arenahippus* tooth enamel appears to respond to ETM2 warming, there is a large amount of variability in the data (average ETM2 $\delta^{18}O \pm 2\sigma$ is 20.6 ± 3.5‰; fig. S4 and table S3), which is also the case during the PETM (24.1 ± 3.5‰) (*10*). This variability likely reflects the impact of aridity on leaf water $\delta^{18}O$ or the impact of multiple seasons of birth on $\delta^{18}O$ of the molar tooth enamel (*46*, *47*).

When comparing ETM2 $\delta^{13}C_{pc}$ records to the observed and predicted M_1 tooth size patterns of *Arenahippus*, it is clear that tooth size exhibits a short-term decrease within the same stratigraphic bounds as ETM2 (Fig. 3C and table S4). Just before the lower stratigraphic boundary of ETM2 (~899 m), the natural log of *Arenahippus* average tooth area (±2σ) is 3.63 ± 0.25 (equal to 37.71 mm^2), which corresponds to an estimated body size of ~7.70 kg (Table 1) (*43*). *Arenahippus* then dwarfs in size by ~14% to an ln(tooth area) of 3.53 ± 0.30 (34.12 mm^2) or ~6.60 kg as the ETM2 CIE peaks around −14‰ $\delta^{13}C_{pc}$. As the CIE recovers to background $\delta^{13}C_{pc}$, *Arenahippus* rebounds ~20% in size to 3.65 ± 0.46 (38.47 mm^2) or ~7.93 kg. The pre-CIE to CIE decrease in *Arenahippus* body size is significant ($P = 0.016$, using a bootstrapping analysis) (see "Statistical analyses").

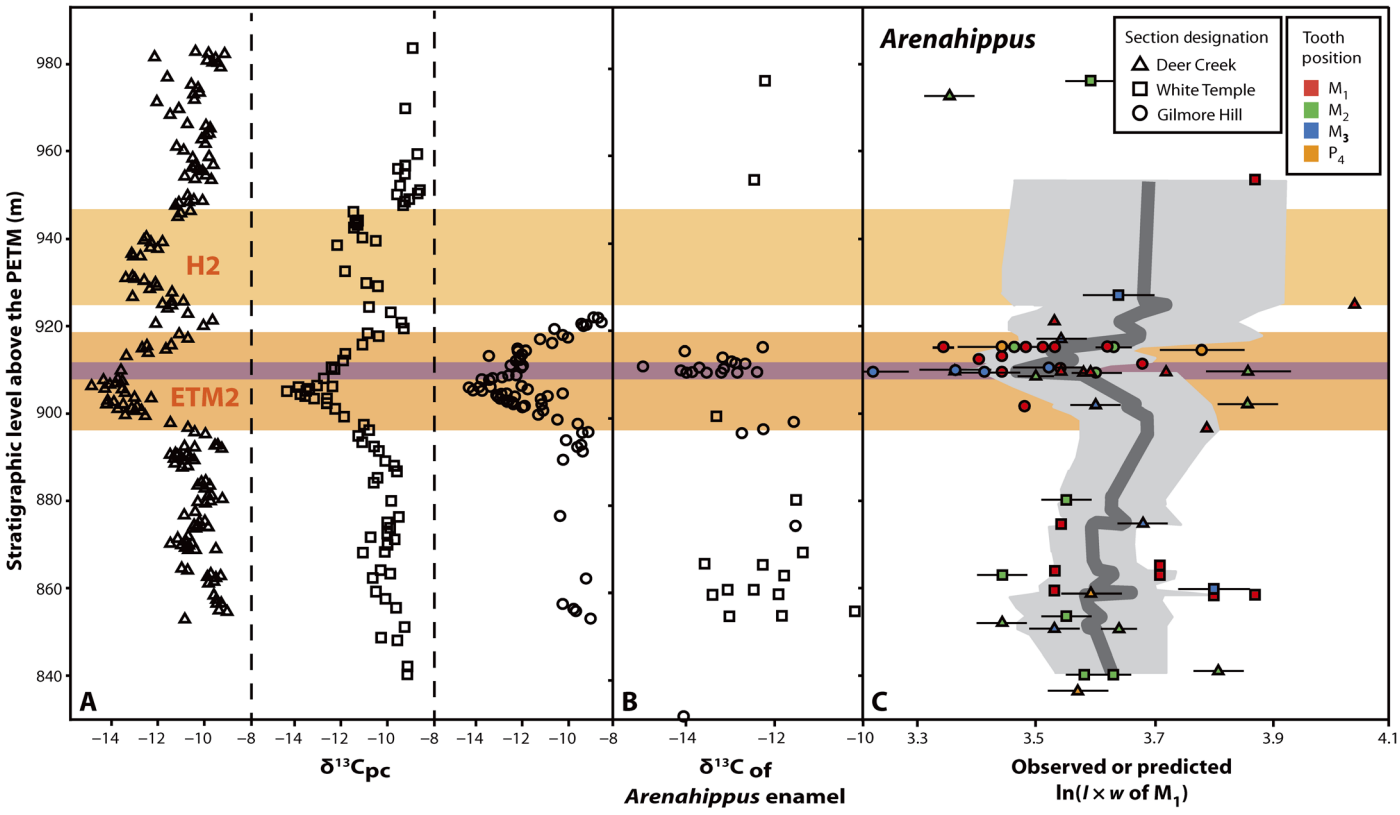

Fig. 3. *Arenahippus* isotopes and tooth size in response to ETM2. Comparison of $\delta^{13}C$ of pedogenic carbonate, $\delta^{13}C$ of *Arenahippus* tooth enamel, and *Arenahippus* tooth size. Orange bands represent body of ETM2 and H2 CIEs. Purple band represents the P2 marker bed. (**A**) Isotopic data from paleosol carbonate nodules. UDC was aligned with GH and WT using the P2 bed (see Fig. 2). *Arenahippus* tooth enamel carbon isotope values (**B**) in association with *Arenahippus* tooth sizes (**C**) were collected across all three McCullough Peaks stratigraphic sections. Tooth size represents the observed M_1 ln(tooth area) or the predicted M_1 value based on tooth size regressions. Dark gray line represents a five-point moving average of all tooth size values, whereas the light gray shaded region represents the 95% CI for the mean. See figure legend for section and tooth position designations. Black horizontal bars on tooth sizes represent propagated analytical error (2σ).

Although data are more limited for *Diacodexis*, *Hyopsodus*, and *Cantius*, both *Diacodexis* and *Cantius* follow similar trends to *Arenahippus* in terms of decrease in body size occurring concordantly with the ETM2 CIE (fig. S5 and table S4). *Diacodexis* shows a statistically significant ($P = 0.010$) pattern very similar to *Arenahippus* between the pre- and mid-ETM2 records, beginning with an average ln(tooth area) of 2.63 ± 0.14 (13.87 mm^2), which corresponds to a body size of 1.62 kg, and then decreasing by ~15% to an average ln(tooth area) of 2.53 ± 0.31 (12.55 mm^2), which corresponds to a body size of 1.37 kg within ETM2 (Table 1). Barring some anomalously small tooth sizes found at the 851- to 852-m level in the *Cantius* data set, these primates show their smallest ln(tooth area) of 2.82 ± 0.18, or 16.78 mm^2 within the peak $\delta^{13}C_{pc}$ values of the ETM2 CIE; however, this change is not significant ($P = 0.315$). *Hyopsodus* exhibits no clear change in body size through ETM2. Pre-ETM2 specimens exhibit an ln(tooth area) of 2.21 ± 0.18, or 9.12 mm^2. *Hyopsodus* then shifts to 2.22 ± 0.25, or 9.21 mm^2, going into mid-ETM2 levels—a scant and statistically insignificant 0.01 natural log unit difference ($P = 0.651$; Table 1). Sample sizes in the post-ETM2 bin were very small ($n = 1$ to 7); thus, the statistical power for these tests is very low. The resulting body size changes from ETM2 to post-ETM2 for all taxa were therefore insignificant. No teeth for any of the studied taxa were found in the H2 CIE; thus, no analyses of body size change across H2 could be performed.

DISCUSSION

Our *Arenahippus* and *Diacodexis* tooth size data demonstrate statistically significant reductions in mammalian body size during ETM2 greenhouse warming as was found during the PETM. With only two early Eocene hyperthermals to compare to date, it is not yet possible to determine an empirical relationship between body size and CIE magnitude. However, it is clear that the smaller ETM2 CIE is associated with less extreme dwarfing, whereas the larger PETM CIE is associated with larger-magnitude body size change, suggesting a monotonic relationship. The dwarfing pattern is shown most clearly by *A. pernix*, the best-sampled taxon in our study ($n = 57$). *Arenahippus* decreases in size by ~14% going into the −3.8‰ ETM2 CIE, which is less than the ~30% decrease in body size going into the −5.9‰ PETM CIE (Fig. 4) (*10*, *14*). The precise percent body size change measured across these hyperthermals partially depends on how the baseline is chosen, but no matter how this is done, the proportional body size change at the PETM is much greater than that at ETM2. Furthermore, given the complex scaling of CIEs detected from pedogenic carbonates compared to marine carbonate (*15*, *48*, *49*), it may be argued that it is instead more appropriate to compare our body size data with the marine surface water records of these CIEs because these come closest to atmospheric carbon isotope changes. In addition, body size changes were driven by environmental changes that were a result of carbon cycle changes of which the carbon isotopes are a derivative and not a direct measure. Either way, our data still suggest a monotonic relationship with the CIE magnitude (Fig. 4).

Table 1. Binned average tooth size and body size estimates across ETM2. Bold *P* values are significant and are based on bootstrapping analyses described in Materials and Methods. *P* values were not determined for $n < 5$ [not applicable (N/A)].

Taxon	Bin	Sample size (*n*)	Average tooth size [ln(*l* × *w*)]	95% Confidence interval*	Body size estimate (kg)		Natural log (ln) unit difference	*P* value	% Body size change between bins
	Pre	21	3.63	0.25	7.70	Pre to mid	−0.10	**0.016**	−14.3%
Arenahippus†	Mid	29	3.53	0.30	6.60				
	Post	7	3.65	0.46	7.93	Mid to post	+0.08	0.032	+20.1%
	Pre	21	2.63	0.14	1.62	Pre to mid	−0.10	**0.010**	−15.0%
Diacodexis†‡	Mid	12	2.53	0.31	1.37				
	Post	4	2.71	0.57	1.83	Mid to post	+0.18	N/A	+32.9%
	Pre	23	2.21	0.18	0.78	Pre to mid	+0.01	0.651	+1.94%
Hyopsodus§	Mid	14	2.22	0.25	0.79				
	Post	2	2.06	0.59	0.62	Mid to post	−0.16	N/A	−7.36%
	Pre	22	2.85	0.25	2.51	Pre to mid	−0.03	0.315	−4.26%
Cantius‡¶	Mid	9	2.82	0.18	2.41				
	Post	1	2.77	—	2.22	Mid to post	−0.05	N/A	−7.79%

*Equal to two SDs (2σ). †Body size calculation based on the study of Legendre (*43*), "artiodactyl + perissodactyl" tooth area–body size regression. ‡Post-ETM2 calculations for *Diacodexis* and *Cantius* are based on a single data point. §Body size calculation based on the study of Damuth (*44*), "nonselenodont ungulates" regression. ¶Body size calculation from Gingerich *et al.* (*74*) and Legendre (*43*), "primate" regressions.

Although this study did observe a decrease in body size for *Arenahippus* and *Diacodexis* during ETM2, measurable teeth for all taxa were less abundant in post-ETM2 stratigraphic levels in these sections, making it difficult to derive meaningful post-CIE body size change estimates. Furthermore, *Diacodexis* and *Cantius* first appeared in the Bighorn Basin during the PETM, and their fossils have not yet been reported at high enough resolution to record body size change within the PETM, making pre- to mid-CIE dwarfing comparisons difficult for these taxa. Despite the unavailability of pre- to mid-PETM tooth size data for *Diacodexis* and *Cantius*, it should be noted that their mid- to post-PETM decrease in body size of 10 to 14% is much less than that for *Sifrhippus* (an early equid closely related to *Arenahippus*) at the PETM (*10*). This suggests that their pre- to mid-ETM2 size decrease would have also been quite small (assuming that their post-PETM background size was equivalent to their pre-PETM size). Thus, a smaller decrease in body size for the two lineages in this study is not surprising. *Hyopsodus*' body size did not change significantly going into ETM2, which contradicts the ~46% decrease in body size during the PETM (Table 1 and fig. S5) (*10*); however, this taxon is known from only two specimens before the PETM (*25*); thus, body size estimates across that CIE are very poorly constrained.

Drivers of body size change

Body size change during periods of climate change is commonly seen throughout historical and geological records among mammals and other organisms (*50*). For instance, since the last glacial maximum, body size trends in woodrat (*Neotoma* sp.) populations tracked known temperature fluctuations (smaller body sizes associated with warming) (*51*). A similar trend was observed in historical records of pocket gophers (*Thomomys talpoides*) (*52*). Both studies concluded that body size responses reflected microevolutionary change. Studies of modern animal populations have also yielded similar body size results. Soay sheep (*Ovis aries*), red deer (*Cervus elaphus*), and California squirrels (*Spermophilus beecheyi*) have all exhibited phenotypic responses to climate change (*53*–*55*). The sheep and deer show a decrease in body size in response to increasing temperatures (*53*, *55*), while the squirrels show a decreased body size in response to decreased precipitation (*54*). Secord *et al.* (*10*) suggested that temperature change might have been the strongest driver of body size change in equids during the PETM. Their results show a strong negative correlation between body size and oxygen isotope values (a proxy for atmospheric temperatures) of mammal teeth from various coexisting lineages (*10*). Both body size and oxygen isotope data sets exhibited a slight lag behind the $\delta^{13}C$, suggesting temperature rather than pCO_2 (that is, via plant nutritional quality) was the most direct driver of body size change.

Among the mechanisms proposed for body size change, the prevailing hypotheses often draw on modern observations of Bergmann's rule to argue that homeothermic mammals surviving at higher temperatures and/or lower latitudes generally exhibit a high surface area–to–volume ratio to efficiently release body heat (*50*, *56*). In this way, Bergmann's rule can also help explain why shifts to a smaller body size may be a common response to warming higher-latitude regions. Similar to modern-day observations, a smaller body size across the early Eocene hyperthermal events may have resulted from immigration either of smaller, lower-latitude members of the taxon's population or, as an anagenetic response of the whole lineage—or some combination of the two (*9*, *10*, *26*, *57*, *58*).

Nutrient availability along with, and as a consequence of, rising temperatures and drought, may also have a direct effect on body size. Assuming that a negative CIE equates to high pCO_2, decreased water and nutrient availability associated with increased pCO_2 and temperature levels could limit plant growth and thus the body size of consumers

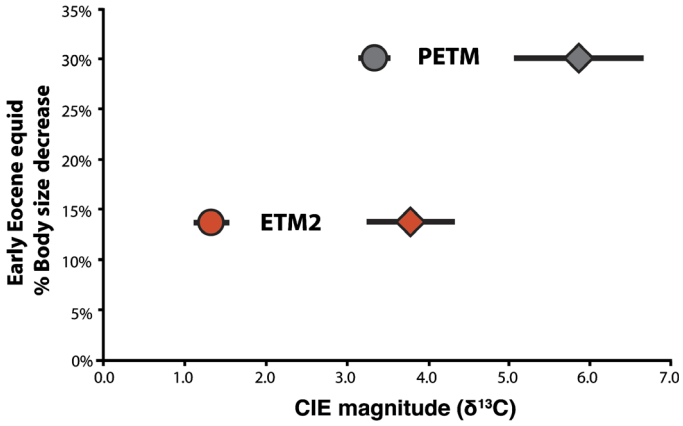

Fig. 4. Relationship between CIE magnitude and dwarfing extent. Body size changes at PETM and ETM2, compared to both marine (circle) and terrestrial (diamond) expressions of the CIEs. Early equids show a decrease in body size of ~30% at the PETM [Secord *et al.* (*10*)], whereas there is only a decrease in size by ~14% at the ETM2. The PETM was a much larger magnitude event at ~3.4 ± 0.1‰ (benthic foraminifera) and ~5.9 ± 0.9‰ (terrestrial) above background $\delta^{13}C$ levels, whereas ETM2 was a smaller-magnitude event at ~1.3 ± 0.2‰ (benthic foraminifera) and ~3.8 ± 0.6‰ (terrestrial) above background $\delta^{13}C$ levels (Abels *et al.* (*15*)].

(*50*). Nutrient availability in soils can be further affected by increasing temperatures, drought, and associated wildfires. This results in soil nitrogen losses, leading to even further reduced plant growth and net primary productivity (*50*, *59*). Ultimately, primary consumers may exhibit a reduction in body size.

Studies of modern lineages of plants, birds, and mammals indicate that reproductive biology, specifically short generation times, may amplify size declines in association with rising temperatures and drought. For instance, drought conditions have been known to lead to smaller offspring (*50*, *60*). Given the close relationship between body size and generation time in mammals, it is possible that as temperatures and/or droughts increase, smaller mammal body size will ensue, followed by shorter generation times, leading to a positive feedback cycle.

Lastly, it is possible that differing precipitation patterns between the two hyperthermal events may have controlled differences in body size change at the events, although the nature of the differing precipitation patterns is not clear. Hydrological records of the PETM suggest more variable and overall drier soils, which are likely linked to precipitation changes (*61*, *62*). Less precipitation may have exacerbated the dwarfing response during the PETM—first in terms of type and quality of consumed vegetation and second in terms of offspring size. In contrast, hydrological records of ETM2 suggest an increase in soil moisture during this event (*15*), perhaps mitigating the dwarfing response. In the same way that the fundamental carbon cycle causes of the PETM and ETM2 may be different (*15*, *63*), the mechanism for body size change at the two events may also be different. However, irrespective of the exact mechanism, it is clear that body size dwarfing in some mammal lineages is closely linked with hyperthermals and may be a common evolutionary response. This suggests that dwarfing will be a likely natural response of some mammals to future global warming.

MATERIALS AND METHODS

Field collection and taxonomic identification

The newly described WT stratigraphic section (base of section at N44.5297712, W108.6757226; top of section at N44.5167142, W108.6720318; WGS 84 datum) and updated component of the GH section (base of updated part of section at N44.521012, W108.650241; top of updated part of section at N44.519680, W108.64923) were measured using a Jacob's staff and Abney level. The tops and bases of individual beds were identified in the section by digging through overlying weathered material to the underlying rock. Each bed was then described in terms of color and grain size.

Carbonate nodules were collected from the WT and GH sections by trenching through the highly weathered overburden into underlying rock until in situ nodules were uncovered. Stacked transects of these trenches spanned a total of >100 m. Nodules were sampled every ~10 to 50 cm within the trenches. Each sample of carbonate nodules was cataloged and noted in relation to the measured stratigraphic section.

Fossil specimens tend to accumulate in surface exposures along small hills and slopes in the McCullough Peaks region. All fossils discovered at WT and GH were recorded with Global Positioning System (GPS) and collected during summer field seasons from 2009 to 2015. UDC fossils were recorded with differential GPS and were collected during the summers of 2010 to 2012. All specimens were measured into the nearest established stratigraphic section and cataloged in the University of Michigan Museum of Paleontology. These data were then transferred to an existing relational database that is used to organize paleontological information. Fossils are often found in situ as they erode out of the outcrop. A study focused within the PETM interval at Polecat Bench in the Bighorn Basin has shown that there is potential for some down-slope movement of fossils after erosion (*64*). The amount of down-slope movement is dependent on variables such as erodibility of the fossil source horizon's rock type and the length in time that the source horizon has been exposed to this erosion. Other factors likely include topographic characteristics such as slope angle (*65*). This down-slope mixing would tend to increase the variance of observed body sizes within stratigraphic horizons and thus dampen any body size patterns that may be observed (*64*).

All specimens that were included in this study were identified as being from within one of the following four species based on the morphological characteristics available: *A. pernix* (*66*), *D. metsiacus* (*67*), *C. abditus* (*68*), and *H. simplex* (*69*). These taxa have been thought to be part of anagenetic lineages that evolved through the early Eocene in the Bighorn Basin and thus are typically referred to as chronospecies (*5*, *7*, *66*, *68*, *70*, *71*). Some disagreement exists over the best taxonomy to use for some of these taxa [for example, see the studies of Froehlich (*72*, *73*)]; however, the morphological continuity of these lineages is well established on the basis of the densely sampled stratigraphic and paleontological record available in the Bighorn Basin (*45*, *66*, *68*, *71*).

Sampling for isotopic analysis

Carbonate nodules were ground flat using a 45–diamond grit lap wheel to sample from the inside of the nodule. Before sampling, the ground surfaces of the carbonate nodules were inspected for signs of alteration (for example, sparry calcite or hematite inclusions). Nodules that were visibly altered were excluded from sampling. Micritic carbonate was ground from the polished nodule surface using a Foredom K.2230 flex shaft rotary drill with diamond tip burrs (~1 to 2 mg of powder was collected from each nodule).

Stable isotope results from *Arenahippus* tooth enamel were used to complement the stable isotopic results from pedogenic carbonates. Isotopic analysis of mammal teeth was restricted to *Arenahippus* because they were the most commonly appearing fossils in mid- to late-Wasatchian

field collections of the McCullough Peaks while also being of a large enough size to yield a sufficient amount of sampling material from each tooth due to the relatively high molar crowns and large tooth area. Isotopic results from tooth enamel were more limited than from carbonate nodules because well-preserved teeth that were conducive to sampling were relatively rare, and the method was destructive; thus, sampling was minimized.

Samples of *Arenahippus* tooth enamel were drilled from cheek teeth of the mandible, producing a sufficient sample size of 3 to 4 mg of enamel powder that was collected after drilling. The P_4, M_1, M_2, and M_3 tooth positions were all sampled on the basis of previous research that suggests there is no systematic isotopic changes across tooth rows (*47*). Teeth with clear signs of alteration, wear, or thin enamel were excluded from analysis. Tooth enamel was drilled with the Foredom K.2230 flex shaft rotary drill with diamond tip burrs. Enamel was removed in vertical strips along the growth axis to average out an intratooth seasonal signal. Modeled after the methods of Koch (*38*), enamel powder was treated with NaOCl followed by 1 M buffered acetic acid (with a pH of ~4.5), both for 24 hours. Before and after the acid treatment, tooth enamel was rinsed five times with deionized water and spun dry in a RevSpin centrifuge for 20 s between each rinse. The final step was to dry samples at 60°C for several hours.

All GH and WT paleosol carbonate and enamel carbonate samples were analyzed at the University of Arizona Environmental Isotope Laboratory with a Finnigan MAT 252 gas-source ratio mass spectrometer with attached Kiel III automatic sample preparation device. The carbonate nodule and enamel powders were reacted with dehydrated phosphoric acid at 70°C, and the final measurement was calibrated through repeated measurements of the NBS 18 and NBS 19 standards. Stable isotope ratio data were reported using "δ" notation, where $\delta = (R_{sample}/R_{standard} - 1) \times 1000$, reported in parts per mil (‰). R stands for the abundance of the heavy to light isotope. On the basis of the standards, the 1σ precision is ±0.1‰ for $\delta^{18}O$ and ±0.1‰ for $\delta^{13}C$.

Body size

Tooth measurements were made on teeth of *Arenahippus*, *Diacodexis*, *Hyopsodus*, and *Cantius*. All teeth were collected from localities stratigraphically spanning ETM2 and H2. Using Fowler-Sylvac Ultra-Cal Mark III digital calipers, the length and width of every tooth crown were measured (in millimeters) three times, and the mean of these measurements was used. Tooth size was converted to body size using a relevant linear regression that is based on the tooth size–body size relationship in all artiodactyls and perissodactyls (*43*), nonselenodont ungulates (*44*), and primates (*43*, *74*).

To compare all tooth positions on the same scale, we normalized non-M_1 tooth area measurements to their predicted M_1 size using tooth size regressions. The predicted M_1 tooth areas were developed from regressions based on all jaws available with M_1 and associated M_2, M_1 and associated M_3, and M_1 and associated P_4 (fig. S6). In certain cases, very few jaws from a particular taxon had both M_1s and associated M_3s or P_4s, etc. In this case, a regression was not formulated, and the other teeth were not used. For instance, a particular taxon may have many M_1s with associated M_2s but very few M_1s with associated M_3s; thus, the M_3 size data were not used. When multiple teeth existed from a single individual (that is, an observed M_1 and/or multiple predicted M_1s), only the observed M_1 was included in the analyzed data set (or the next "best" predicted tooth is used, on the basis of regression strength). When a single individual with both teeth of the same position existed, an average of the tooth size was used.

Statistical analyses

Moving averages with 95% CIs were calculated for tooth size data within each lineage to identify stratigraphic patterns. The natural log of each observed and predicted M_1 was plotted against a stratigraphic level. A five-point running mean of tooth size was then applied across the stratigraphic intervals. If multiple teeth occurred at the same stratigraphic interval, then an average of the teeth was taken before the application of the running mean. Upper and lower 95% CIs were then applied to the five-point moving average values.

A simple binning technique was used to calculate the average tooth size, and thus average body size, change across the CIEs. Teeth were determined to be within a CIE if they came from stratigraphic levels with paleosol carbonate $\delta^{13}C$ values of less than −11.5‰. This cutoff value was based on a natural gap in the $\delta^{13}C$ data that lies approximately halfway between the lowest CIE $\delta^{13}C$ value (−14.3‰) and highest background $\delta^{13}C$ value (−8.6‰). As a result, the ETM2 CIE falls between 900 and 915 m above the PETM, and H2 falls between 932 and 939 m. Note that only two paleosol carbonate values represented the H2 CIE given this criterion, and no tooth specimens from any taxa in our study fell within this limited stratigraphic range.

The natural autocorrelation of tooth size data throughout a lineage made it difficult to apply standard statistical analyses; thus, a bootstrapping approach was used here instead. Tooth size data from each lineage were bootstrapped to determine whether pre-CIE tooth sizes were significantly different from CIE tooth sizes and whether CIE tooth sizes were significantly different from post-CIE tooth sizes. Tooth size data from each lineage were binned into pre-CIE, CIE, and post-CIE groups according to the criterion outlined above. The number of tooth size data points in each bin was determined for a given lineage ($n_{pre\text{-}CIE}$, n_{CIE}, and $n_{post\text{-}CIE}$). The original data set for each lineage was then resampled with replacement (bootstrapped) 1000 times, creating subsamples with the same $n_{pre\text{-}CIE}$, n_{CIE}, and $n_{Post\text{-}CIE}$ as the original sample. At each iteration, the difference was calculated between the means of the bootstrapped subsamples. The distribution of the differences between the means of the bootstrapped subsamples was then used to determine the significance of the observed difference between the means of the pre-CIE, CIE, and post-CIE tooth size subsamples. Observed differences falling in a 2.5% tail of the bootstrapped distribution were considered significant. No teeth for any of the studied taxa were found in the H2 CIE; thus, this approach could not be used to study the hyperthermal.

SUPPLEMENTARY MATERIALS

Supplementary material for this article is available at http://advances.sciencemag.org/cgi/content/full/3/3/e1601430/DC1

fig. S1. Section localities.
fig. S2. Photos of P2 marker bed.
fig. S3. Updated GH section.
fig. S4. Stable isotopes of *Arenahippus* tooth enamel.
fig. S5. ETM2 dwarfing patterns of *Arenahippus*, *Diacodexis*, *Hyopsodus*, and *Cantius*.
fig. S6. Tooth size regression analyses.
table S1. WT carbonate nodule $\delta^{13}C$.
table S2. Updated GH carbonate nodule $\delta^{13}C$.
table S3. Carbon and oxygen isotope data of *Arenahippus* tooth specimens.
table S4. Stratigraphic levels and tooth size observations associated with each specimen in this study.

REFERENCES AND NOTES

1. H. A. Aziz, F. J. Hilgen, G. M. van Luijk, A. Sluijs, M. J. Kraus, J. M. Pares, P. D. Gingerich, Astronomical climate control on paleosol stacking patterns in the upper Paleocene–lower Eocene Willwood Formation, Bighorn Basin, Wyoming. *Geology* **36**, 531–534 (2008).

2. F. A. McInerney, S. L. Wing, The Paleocene-Eocene thermal maximum: A perturbation of carbon cycle, climate, and biosphere with implications for the future. *Annu. Rev. Earth Planet. Sci.* **39**, 489–516 (2011).
3. A. Sluijs, S. Schouten, M. Pagani, M. Woltering, H. Brinkhuis, J. S. Sinninghe Damsté, G. R. Dickens, M. Huber, G.-J. Reichart, R. Stein, J. Matthiessen, L. J. Lourens, N. Pedentchouk, J. Backman, K. Moran; Expedition 302 Scientists, Subtropical Arctic Ocean temperatures during the Palaeocene/Eocene thermal maximum. *Nature* **441**, 610–613 (2006).
4. J. W. H. Weijers, S. Schouten, A. Sluijs, H. Brinkhuis, J. S. Sinninghe Damsté, Warm arctic continents during the Palaeocene–Eocene thermal maximum. *Earth Planet. Sci. Lett.* **261**, 230–238 (2007).
5. H. C. Fricke, W. C. Clyde, J. R. O'Neil, P. D. Gingerich, Evidence for rapid climate change in North America during the latest Paleocene thermal maximum: Oxygen isotope compositions of biogenic phosphate from the Bighorn Basin (Wyoming). *Earth Planet. Sci. Lett.* **160**, 193–208 (1998).
6. H. C. Fricke, S. L. Wing, Oxygen isotope and paleobotanical estimates of temperature and $\delta^{18}O$–latitude gradients over North America during the early Eocene. *Am. J. Sci.* **304**, 612–635 (2004).
7. P. D. Gingerich, New earliest Wasatchian mammalian fauna from the Eocene of northwestern Wyoming: Composition and diversity in a rarely sampled high-floodplain assemblage. *Univ. Mich. Pap. Paleontol.* **28**, 37–71 (1989).
8. W. C. Clyde, P. D. Gingerich, Mammalian community response to the latest Paleocene thermal maximum: An isotaphonomic study in the northern Bighorn Basin, Wyoming. *Geology* **26**, 1011–1014 (1998).
9. P. D. Gingerich, Mammalian responses to climate change at the Paleocene-Eocene boundary: Polecat Bench record in the northern Bighorn Basin, Wyoming, *Spec. Pap. Geol. Soc. Am.* **369**, 463–478 (2003).
10. R. Secord, J. I. Bloch, S. G. B. Chester, D. M. Boyer, A. R. Wood, S. L. Wing, M. J. Kraus, F. A. McInerney, J. Krigbaum, Evolution of the earliest horses driven by climate change in the Paleocene-Eocene thermal maximum. *Science* **335**, 959–962 (2012).
11. K. D. Rose, A. E. Chew, R. H. Dunn, M. J. Kraus, H. C. Fricke, S. P. Zack, Earliest Eocene mammalian fauna from the Paleocene–Eocene Thermal Maximum at Sand Creek Divide, southern Bighorn Basin. *Univ. Mich. Pap. Paleontol.* **36**, 1–122 (2012).
12. L. J. Lourens, A. Sluijs, D. Kroon, J. C. Zachos, E. Thomas, U. Röhl, J. Bowles, I. Raffi, Astronomical pacing of late Palaeocene to early Eocene global warming events. *Nature* **435**, 1083–1087 (2005).
13. L. Stap, L. J. Lourens, E. Thomas, A. Sluijs, S. Bohatyand, J. C. Zachos, High-resolution deep-sea carbon and oxygen isotope records of Eocene thermal maximum 2 and H2. *Geology* **38**, 607–610 (2010).
14. H. A. Abels, W. C. Clyde, P. D. Gingerich, F. J. Hilgen, H. C. Fricke, G. J. Bowen, L. J. Lourens, Terrestrial carbon isotope excursions and biotic change during Palaeogene hyperthermals. *Nat. Geosci.* **5**, 326–329 (2012).
15. H. A. Abels, V. Lauretano, A. van Yperen, T. Hopman, J. C. Zachos, L. J. Lourens, P. D. Gingerich, G. J. Bowen, Carbon isotope excursions in paleosol carbonate marking five early Eocene hyperthermals in the Bighorn Basin, Wyoming. *Clim. Past Discuss.* **11**, 1857–1885 (2016).
16. A. E. Chew, Mammal faunal change in the zone of the Paleogene hyperthermals ETM2 and H2. *Clim. Past Discuss.* **11**, 1223–1237 (2015).
17. A. R. D'Ambrosia, W. C. Clyde, H. C. Fricke, K. E. Snell, P. D. Gingerich, Repetitive mammalian dwarfism associated with early Eocene carbon cycle perturbations. *Rend. Online Soc. Geol. It.* **31**, 52–53 (2014).
18. P. D. Gingerich, Biostratigraphy of the continental Paleocene-Eocene boundary interval on Polecat bench in the northern Bighorn Basin. *Univ. Mich. Pap. Paleontol.* **33**, 37–71 (2001).
19. T. M. Bown, K. D. Rose, E. L. Simons, S. L. Wing, "Distribution and stratigraphic correlation of upper Paleocene and lower Eocene fossil mammal and plant localities of the Fort Union, Willwood, and Tatman formations, Southern Bighorn Basin, Wyoming" (USGS Professional Paper 1540, 1994).
20. M. J. Kraus, Sedimentology and depositional setting of the Willwood formation in the Bighorn and Clarks Fork basins. *Univ. Mich. Pap. Paleontol.* **33**, 15–28 (2001).
21. T. M. Bown, M. J. Kraus, Integration of channel and floodplain suites. I. Developmental sequence and lateral relations of alluvial paleosols. *J. Sediment. Res.* **57**, 587–601 (1987).
22. R. Secord, S. L. Wing, A. Chew, Stable isotopes in early Eocene mammals as indicators of forest canopy structure and resource partitioning. *Paleobiology* **34**, 282–300 (2008).
23. J. Zachos, M. Pagani, L. Sloan, E. Thomas, K. Billups, Trends, rhythms, and aberrations in global climate 65 Ma to present. *Science* **292**, 686–693 (2001).
24. K. E. Snell, B. L. Thrasher, J. M. Eiler, P. L. Koch, L. C. Sloan, N. J. Tabor, Hot summers in the Bighorn Basin during the early Paleogene. *Geology* **41**, 55–58 (2013).
25. K. D. Rose, The Clarkforkian land-mammal age and mammalian faunal composition across the Paleocene-Eocene boundary. *Univ. Mich. Pap. Paleontol.* **26**, 1–115 (1981).
26. P. Gingerich, Environment and evolution through the Paleocene–Eocene thermal maximum. *Trends Ecol. Evol.* **21**, 246–253 (2006).
27. P. L. Koch, J. C. Zachos, D. L. Dettman, Stable isotope stratigraphy and paleoclimatology of the Paleogene Bighorn Basin (Wyoming, USA). *Palaeogeogr. Palaeoclimatol. Palaeoecol.* **115**, 61–89 (1995).
28. G. J. Bowen, P. L. Koch, P. D. Gingerich, D. Norris, S. Bains, R. M. Corfield, Refined isotope stratigraphy across the continental Paleocene Eocene boundary on Polecat Bench in the northern Bighorn Basin. *Univ. Mich. Pap. Paleontol.* **33**, 73–88 (2001).
29. G. J. Bowen, B. J. Maibauer, M. J. Kraus, U. Röhl, T. Westerhold, A. Steimke, P. D. Gingerich, S. L. Wing, W. C. Clyde, Two massive, rapid releases of carbon during the onset of the Palaeocene–Eocene thermal maximum. *Nat. Geosci.* **8**, 44–47 (2014).
30. P. L. Koch, Isotopic reconstruction of past continental environments. *Annu. Rev. Earth Planet. Sci.* **26**, 573–613 (1998).
31. P. L. Koch, W. C. Clyde, R. P. Hepple, M. L. Fogel, S. L. Wingand, J. C. Zachos, Carbon and oxygen isotope records from paleosols spanning the Paleocene-Eocene boundary, Bighorn Basin, Wyoming. *Spec. Pap. Geol. Soc. Am.* **369**, 49–64 (2003).
32. G. D. Farquhar, M. H. O'Leary, J. A. Berry, On the relationship between carbon isotope discrimination and the intercellular carbon dioxide concentration in leaves. *Funct. Plant Biol.* **9**, 121–137 (1982).
33. G. D. Farquhar, J. R. Ehleringer, K. T. Hubick, Carbon isotope discrimination and photosynthesis. *Annu. Rev. Plant Biol.* **40**, 503–537 (1989).
34. P. N. Pearson, M. R. Palmer, Atmospheric carbon dioxide concentrations over the past 60 million years. *Nature* **406**, 695–699 (2000).
35. J. Daniel Bryant, P. N. Froelich, A model of oxygen isotope fractionation in body water of large mammals. *Geochim. Cosmochim. Acta* **59**, 4523–4537 (1995).
36. M. J. Kohn, Predicting animal $\delta^{18}O$: Accounting for diet and physiological adaptation. *Geochim. Cosmochim. Acta* **60**, 4811–4829 (1996).
37. D. W. Podlesak, A.-M. Torregrossa, J. R. Ehleringer, M. Denise Dearing, B. H. Passey, T. E. Cerling, Turnover of oxygen and hydrogen isotopes in the body water, CO_2, hair, and enamel of a small mammal. *Geochim. Cosmochim. Acta* **72**, 19–35 (2008).
38. P. L. Koch, The effects of sample treatment and diagenesis on the isotopic integrity of carbonate in biogenic hydroxylapatite. *J. Archaeol. Sci.* **24**, 417–429 (1997).
39. M. J. Kohn, T. E. Cerling, Stable isotope compositions of biological apatite. *Rev. Mineral. Geochem.* **48**, 455–488 (2002).
40. M. H. O'Leary, Carbon isotopes in photosynthesis. *BioScience* **38**, 328–336 (1988).
41. A. Longinelli, Oxygen isotopes in mammal bone phosphate: A new tool for paleohydrological and paleoclimatological research? *Geochim. Cosmochim. Acta* **48**, 385–390 (1984).
42. P. D. Gingerich, Size variability of the teeth in living mammals and the diagnosis of closely related sympatric fossil species. *J. Paleontol.* **48**, 895–903 (1974).
43. S. Legendre, Analysis of mammalian communities from the late Eocene and Oligocene of southern France. *Palaeovertebrata* **16**, 191–212 (1986).
44. J. Damuth, in *Body Size in Mammalian Paleobiology: Estimation and Biological Implications* (Cambridge Univ. Press, 1990), pp. 229–253.
45. K. D. Rose, *The Beginning of the Age of Mammals* (JHU Press, 2006).
46. N. E. Levin, T. E. Cerling, B. H. Passey, J. M. Harris, J. R. Ehleringer, A stable isotope aridity index for terrestrial environments. *Proc. Natl. Acad. Sci. U.S.A.* **103**, 11201–11205 (2006).
47. A. R. D'Ambrosia, W. C. Clyde, H. C. Fricke, A. E. Chew, Stable isotope patterns found in early Eocene equid tooth rows of North America: Implications for reproductive behavior and paleoclimate. *Palaeogeogr. Palaeoclimatol. Palaeoecol.* **414**, 310–319 (2014).
48. F. A. Smith, S. L. Wing, K. H. Freeman, Magnitude of the carbon isotope excursion at the Paleocene-Eocene thermal maximum: The role of plant community change. *Earth Planet. Sci. Lett.* **262**, 50–65 (2007).
49. B. A. Schubert, A. Hope Jahren, Reconciliation of marine and terrestrial carbon isotope excursions based on changing atmospheric CO_2 levels. *Nat. Commun.* **4**, 1653 (2013).
50. J. A. Sheridan, D. Bickford, Shrinking body size as an ecological response to climate change. *Nat. Clim. Chang.* **1**, 401–406 (2011).
51. F. A. Smith, J. L. Betancourt, J. H. Brown, Evolution of body-size in the woodrat over the past 25,000 years of climate change. *Science* **270**, 2012–2014 (1995).
52. E. A. Hadly, M. H. Kohn, J. A. Leonard, R. K. Wayne, A genetic record of population isolation in pocket gophers during Holocene climatic change. *Proc. Natl. Acad. Sci. U.S.A.* **95**, 6893–6896 (1998).
53. E. Post, N. C. Stenseth, R. Langvatn, J.-M. Fromentin, Global climate change and phenotypic variation among red deer cohorts. *Proc. R. Soc. Lond. B Biol. Sci.* **264**, 1317–1324 (1997).
54. J. L. Blois, R. S. Feranec, E. A. Hadly, Environmental influences on spatial and temporal patterns of body-size variation in California ground squirrels (*Spermophilus beecheyi*). *J. Biogeogr.* **35**, 602–613 (2008).
55. A. Ozgul, S. Tuljapurkar, T. G. Benton, J. M. Pemberton, T. H. Clutton-Brock, T. Coulson, The dynamics of phenotypic change and the shrinking sheep of St. Kilda. *Science* **325**, 464–467 (2009).
56. J. L. Gardner, A. Peters, M. R. Kearney, L. Joseph, R. Heinsohn, Declining body size: A third universal response to warming? *Trends Ecol. Evol.* **26**, 285–291 (2011).

57. B. J. Burger, Northward range extension of a diminutive-sized mammal (*Ectocion parvus*) and the implication of body size change during the Paleocene–Eocene Thermal Maximum. *Palaeogeogr. Palaeoclimatol. Palaeoecol.* **363–364**, 144–150 (2012).
58. B. D. Rankin, J. W. Fox, C. R. Barrón-Ortiz, A. E. Chew, P. A. Holroyd, J. A. Ludtke, X. Yang, J. M. Theodor, The extended Price equation quantifies species selection on mammalian body size across the Palaeocene/Eocene Thermal Maximum. *Proc. Biol. Sci.* **282**, 20151097 (2015).
59. P. M. Vitousek, J. R. Gosz, C. C. Grier, J. M. Melillo, W. A. Reiners, A comparative analysis of potential nitrification and nitrate mobility in forest ecosystems. *Ecol. Monogr.* **52**, 155–177 (1982).
60. S. J. Franks, A. E. Weis, A change in climate causes rapid evolution of multiple life-history traits and their interactions in an annual plant. *J. Evol. Biol.* **21**, 1321–1334 (2008).
61. M. J. Kraus, F. A. McInerney, S. L. Wing, R. Secord, A. A. Baczynski, J. I. Bloch, Paleohydrologic response to continental warming during the Paleocene–Eocene Thermal Maximum, Bighorn Basin, Wyoming. *Palaeogeogr. Palaeoclimatol. Palaeoecol.* **370**, 196–208 (2013).
62. M. J. Kraus, D. T. Woody, J. J. Smith, V. Dukic, Alluvial response to the Paleocene–Eocene Thermal Maximum climatic event, Polecat Bench, Wyoming (U.S.A.). *Palaeogeogr. Palaeoclimatol. Palaeoecol.* **435**, 177–192 (2015).
63. S. Kirtland Turner, P. F. Sexton, C. D. Charles, R. D. Norris, Persistence of carbon release events through the peak of early Eocene global warmth. *Nat. Geosci.* **7**, 748–751 (2014).
64. A. R. Wood, M. J. Kraus, P. D. Gingerich, Downslope fossil contamination: Mammal-bearing fluvial conglomerates and the Paleocene-Eocene Faunal Transition (Willwood formation, Bighorn Basin, Wyoming). *Palaios* **23**, 380–390 (2008).
65. J. W. Rick, Downslope movement and archaeological intrasite spatial analysis. *Am. Antiq.* **41**, 133–144 (1976).
66. P. D. Gingerich, Systematics and evolution of early Eocene Perissodactyla (Mammalia) in the Clarks Fork Basin, Wyoming. *Contrib. Mus. Paleontol. Univ. Mich.* **28**, 181–213 (1991).
67. M. C. McKenna, Fossil Mammalia from the early Wasatchian Four Mile fauna, Eocene of northwest Colorado. *Univ. Calif. Publ. Geol. Sci.* **37**, 1–130 (1960).
68. P. D. Gingerich, R. A. Haskin, Dentition of early Eocene Pelycodus jarrovii (Mammalia, Primates) and the generic attribution of species formerly referred to Pelycodus. *Contrib. Mus. Paleontol. Univ. Mich.* **25**, 327–337 (1981).
69. F. B. Loomis, Hyopsodidae of the Wasatch and Wind River basins. *Am. J. Sci.* **114**, 416–424 (1905).
70. P. D. Gingerich, E. L. Simons, Systematics, phylogeny, and evolution of early Eocene Adapidae (Mammalia, Primates) in North America. *Contrib. Mus. Paleontol. Univ. Mich.* **24**, 245–279 (1977).
71. P. D. Gingerich, New species of Apheliscus, Haplomylus, and Hyopsodus (Mammalia, Condylarthra) from the late Paleocene of southern Montana and early Eocene of northwestern Wyoming. *Contrib. Mus. Paleontol. Univ. Mich.* **29**, 119–134 (1994).
72. D. J. Froehlich, Quo vadis eohippus? The systematics and taxonomy of the early Eocene equids (Perissodactyla). *Zool. J. Linn. Soc.* **134**, 141–256 (2002).
73. D. J. Froehlich, Phylogenetic systematics of basal perissodactyls. *J. Vertebr. Paleontol.* **19**, 140–159 (1999).
74. P. D. Gingerich, B. H. Smith, K. Rosenberg, Allometric scaling in the dentition of primates and prediction of body weight from tooth size in fossils. *Am. J. Phys. Anthropol.* **58**, 81–100 (1982).

Acknowledgments: We thank field assistants over several field seasons, including T. Amaral, J.-F. Benoit, D. Conwell, S. Jech, J. Riedel, K. Tsukui, G. Welter, J. M. Krause, and A. Jacobsen. We also thank K. Steensma, S. Hilgen, S. Hilgen, S. Hilgen, F. Hilgen, N. de Winter, M. Gingerich, D. Gingerich, F. van den Berg, S. Smeets, P. van den Bern, A. van Yperen, and the Michigan crew for fossil hunting across UDC. We also thank R. Secord and A. Wood for input and advice. We are indebted to the Churchill family of Powell, WY. Sample analyses were carried out by D. Dettman at the University of Arizona Environmental Isotope Laboratory. We thank L. van den Hoek Ostende and one anonymous reviewer for their constructive reviews of the manuscript. **Funding:** This project was supported by a grant to W.C.C. and P.D.G. from the NSF (EAR0958821). A.R.D. was funded by two Geological Society of America Graduate Research Grants, a Paleontological Society Student Research Grant, and a Sigma Xi Grant-in-Aid. H.A.A. was supported by the Nederlandse Organisatie voor Wetenschappelijk Onderzoek (VENI grant 863.11.006). Fossils were collected under U.S. Bureau of Land Management permit 100-WY-PA94. **Author contributions:** A.R.D., W.C.C., and H.C.F. designed the project. All authors contributed to the fieldwork. H.A.A. provided the UDC data. P.D.G. provided access to University of Michigan fossil specimens. A.R.D. performed background research and data analysis. All authors contributed to the interpretation of results. A.R.D. prepared the manuscript, and all of the authors reviewed and edited it. **Competing interests:** The authors declare that they have no competing interests. **Data and materials availability:** All data needed to evaluate the conclusions in the paper are present in the paper and/or the Supplementary Materials. Additional data related to this paper may be requested from the authors.

Submitted 23 June 2016
Accepted 3 February 2017
Published 15 March 2017
10.1126/sciadv.1601430

Citation: A. R. D'Ambrosia, W. C. Clyde, H. C. Fricke, P. D. Gingerich, H. A. Abels, Repetitive mammalian dwarfing during ancient greenhouse warming events. *Sci. Adv.* **3**, e1601430 (2017).